Sensory Feedback in a Half-Center Oscillator Model

Mario F. Simoni*, *Member, IEEE*, and Stephen P. DeWeerth, *Senior Member, IEEE*

***Abstract*—We hypothesize that one role of sensorimotor feedback for rhythmic movements in biological organisms is to synchronize the frequency of movements to the mechanical resonance of the body. Our hypothesis is based on recent studies that have shown the advantage of moving at mechanical resonance and how such synchronization may be possible in biology. We test our hypothesis by developing a physical system that consists of a silicon-neuron central pattern generator (CPG), which controls the motion of a beam, and position sensors that provide feedback information to the CPG. The silicon neurons that we use are integrated circuits that generate neural signals based on the Hodgkin-Huxley dynamics. We use this physical system to develop a model of the interaction between the sensory feedback and the complex dynamics of the neurons to create the closed-loop system behavior. This model is then used to describe the conditions under which our hypothesis is valid and the general effects of sensorimotor feedback on the rhythmic movements of this system.**

***Index Terms*—Central pattern generators, rhythmic movements, sensorimotor feedback, silicon neurons.**

I. Introduction

FEEDBACK is an essential part of any effective control system, including neural systems. Animals are capable of interacting with their environments through complex coordinated movements that would be impossible without some form of feedback. In particular, rhythmic movements, such as walking, swimming, and breathing, comprise a large portion of the movements made by animals. Central pattern generators (CPGs) are groups of interconnected neurons that can produce rhythmic electrical patterns that underlie such movements. It is clear that CPGs must be influenced by sensorimotor feedback to compensate for changing environments, however the exact nature of this interaction is still unclear [1].

We hypothesize that an additional purpose of sensory feedback for rhythmic movements is to synergize the nervous and musculoskeletal systems so that the resulting frequency of movement is related to the body's mechanical resonance. There are several advantages for matching this mechanical resonance: conservation of energy, reduction of jitter during movements, and improvement of cycle-to-cycle repeatability [2], [3]. Modeling studies have been done recently to understand the role of sensory feedback and mechanical resonance in biological systems [4]–[7]. However, one factor that was not addressed thoroughly in these studies was the complex nonlinear dynamics of the neurons.

We are developing silicon neurons that can create complex neural dynamics in real time and with very low power consumption, and we have previously used them to implement a CPG [8], [9]. Because of these properties of the silicon neurons, we have long term goals of using them as controllers for autonomous machines and in biomedical technologies such as implantable neural stimulators and funtional electrical stimulation (FES). In addition to testing our hypothesis, this work is a study of how these silicon neurons will behave in the context of a closed-loop system.

To test our hypothesis we have implemented a closed-loop model of biological rhythmic movement control that is based on a silicon neuron CPG. The properties of these silicon neurons make it possible to study such a system with complex neural dynamics while it operates in real time and in a real-world environment. We believe that studying a physical model will provide insights that would be more difficult to obtain from computer simulations alone because of the ability to tweak parameters and immediately observe the effects. Our study of this system has led to the development of a model that can describe the relationship between sensory feedback, mechanics, and neural pattern generator and how that relationship creates the steady-state system frequency.

II. Implementation of the Closed-Loop System

The closed-loop system that we implemented is a generic model of biological rhythmic movement control about a joint or body segment that has a single mechanical degree-of-freedom. Fig. 1 shows both a high-level block diagram and the physical implementation of this system. A CPG excites a pair of antagonistic muscles that move the limb or body segment from side to side. To close the loop, the CPG receives proprioceptive feedback from position sensors.

When implementing the physical system we chose to emulate some of the components in software to provide greater flexibility. Fig. 1(B) shows that the calculation of the total force acting on the mass and the total synaptic current for each of the neurons are implemented as numerical simulations of mathematical models running on a real-time control board. The hardware components are the silicon neurons and a physical mass, which was used so that we did not have to simulate the nonidealities of operating in a real-world environment. Consequently, a dc electric motor was used to provide the forces that acted on the mass. The interaction between simulation and hardware components is done via the real-time control board, which also facilitates the changing of parameters while the system is operating. As such, we could easily adjust parameters such as the mechanical resonant frequency to test our hypothesis.

Manuscript received June 3, 2005; revised July 22, 2006. This work was supported in part by the National Science Foundation (NSF) under Grant IBN-9872759 and in part by the NSF-sponsored Telluride Neuromorphic-Engineering Workshop. *Asterisk indicates corresponding author.*

*M. F. Simoni is with the Rose-Hulman Institute of Technology, 5500 Wabash Ave., Terre Haute, IN 47803 USA (e-mail: simoni@rose-hulman.edu).

S. P. DeWeerth is with the Georgia Institute of Technology, Atlanta, GA 30332 USA (e-mail: steve.deweerth@ece.gatech.edu).

Color versions of Figs. 4–8 and 10 are available online at http://ieeexplore.ieee.org.

Digital Object Identifier 10.1109/TBME.2006.886868

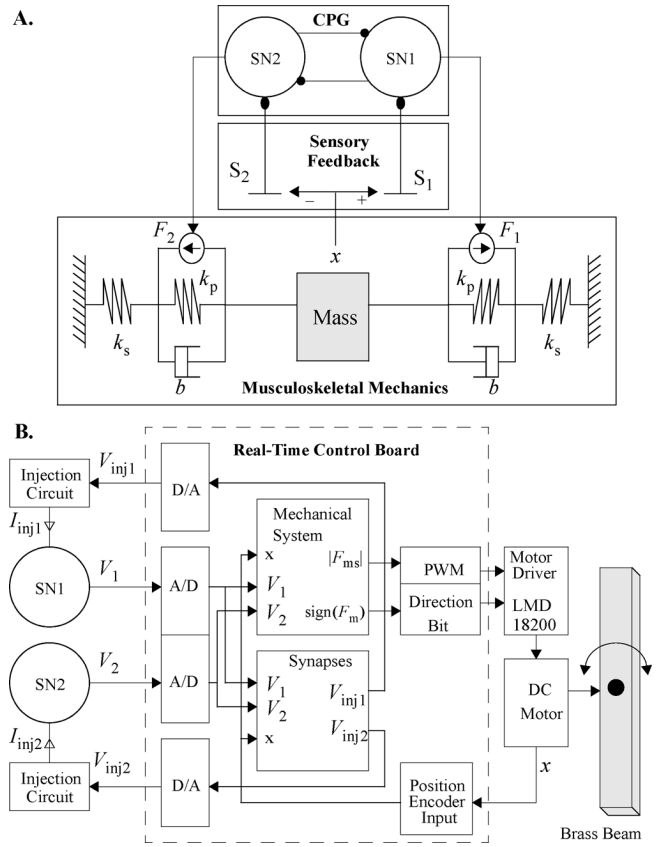

Fig. 1. Two representations of the closed-loop system. (A) A high level block diagram of the closed-loop system. The silicon neurons are SN1(2) and the solid dots represent inhibitory synapses. The position sensors are shown as $S_{1(2)}$. The "musculoskeletal mechanics" block represents a pair of antagonistic muscles acting about a joint. The active force production of the muscles is modeled as $F_{1(2)}$, and the passive properties of the musculoskeletal system are represented with the mass, springs, and dampers. (B) A schematic of the physical implementation in A. The real-time control board implements the mathematical models of the musculoskeletal mechanics and the synapses. The inputs to this board are the membrane potentials of the two silicon neurons, $V_{1(2)}$, and the position sensor from the shaft of the electric motor, x. The outputs of the board are the voltages that represent the total synaptic current into each silicon neuron, $V_{\mathrm{inj}1(2)}$, and the signals that encode the torque and direction of the electric motor.

A. Implementing the CPG With Silicon Neurons

The CPG consists of two neurons with reciprocal inhibition (a half-center oscillator), which is the simplest configuration that can produce two distinct electrical patterns with a given phase relationship for exciting antagonistic muscles. The reciprocal inhibition produces this pattern by causing one of the neurons to be inhibited while the other is spiking. The neurons reverse states according to the interaction between the individual neuron dynamics and the dynamics of the reciprocal inhibition.

The CPG was implemented with a pair of silicon neurons, for which typical bursting patterns are shown in Fig. 2. We showed previously that the silicon neurons faithfully implement the dynamics of the Hodgkin–Huxley formalism (see Appendix for equations that describe the dynamics of the silicon neuron), and that the CPG is capable of producing a wide variety of bursting behaviors as the model parameters are varied. The silicon neurons that we used for this work contain a set of voltage-dependent conductances that were based on a mathematical model of the leech heart interneuron (HN) [10]. We used this model be-

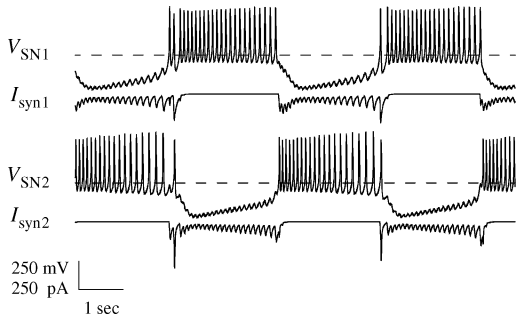

Fig. 2. Bursting at the canonical parameter values. The time series show both the membrane potentials and the synaptic currents of the two silicon neurons in the half-center oscillator. The dashed lines that are associated with the membrane potentials represent the synaptic threshold voltage. The flat regions of the synaptic currents represent $I_{\mathrm{syn}} = 0$.

cause the HN neuron exhibits a wide variety of robust bursting behaviors and because the mathematical model has been extensively verified through experimental studies [11]. In addition to a leak conductance, g_{leak}, each silicon neuron has six voltage-dependent conductances: 1) g_{Na}, a fast sodium conductance with inactivation, 2) g_{P}, a persistent sodium conductance with activation only, 3) g_{K1}, a fast potassium conductance that also inactivates, 4) g_{K2}, a slower potassium conductance with activation only, 5) g_{Ca}, a slow calcium conductance with inactivation, and 6) g_{h} a hyperpolarization activated conductance. For each of these conductances, we can control independently the reversal potentials, maximal conductances, activation/inactivation time constants, and activation/inactivation half-maximal potentials. The slopes of the activation/inactivation functions are fixed at biological values.

The reciprocal inhibitory synapses of this CPG were implemented with a combination of hardware and software. The real-time control board computed the value of the synaptic currents based on the measured membrane potential of each neuron. The board then output these values as voltages that were converted to currents using standard operational amplifier circuits (see V_{inj} and I_{inj} in Fig. 1). We chose a mathematical synapse model that could be implemented relatively easily with analog integrated circuits in the future. This model contains a single state variable and is based on the alpha function [12]

$$I_{\mathrm{syn}} = \bar{g}_{\mathrm{syn}} n (E_{\mathrm{syn}} - V) \tag{1a}$$

where I_{syn} is the post-synaptic current, $\bar{g}_{\mathrm{syn}}$ is the maximal synaptic conductance, $n \in [0,1]$ is the activation state variable, E_{syn} is the synaptic reversal potential, and V is the post-synaptic membrane potential. The dynamics of the activation variable, n, are given by

$$\frac{dn}{dt} = \frac{1}{\tau_n}(n_\infty(V_{\mathrm{pre}}) - n) \tag{1b}$$

where τ_n is the time constant, $n_\infty(V_{\mathrm{pre}})$ is the steady-state value of n as a function of the pre-synaptic membrane potential, V_{pre}. The steady-state function of n is given by

$$n_\infty(V_{\mathrm{pre}}) = \begin{cases} 0, & \text{if } V_{\mathrm{pre}} \le V_{\mathrm{th}} \\ \tanh(S_n(V_{\mathrm{pre}} - V_{\mathrm{th}})), & \text{if } V_{\mathrm{pre}} > V_{\mathrm{th}} \end{cases} \tag{1c}$$

where $V_{\rm th}$ is the threshold voltage for the action potential and S_n is the slope of the steady-state activation function. Equation (1b) is a first order ODE that produces the exponential rise and fall of the alpha function. The synaptic currents for the reciprocal inhibition to each silicon neuron are also shown in Fig. 2.

B. Implementing the Mechanical System

The mechanical system, as shown in Fig. 1, models an antagonistic muscle pair and the passive properties of the musculoskeletal system. The real-time control board computed the total force acting on the mass based on a mathematical model of the mechanical system, the measured position of the mass, and the activity of the CPG. This total force value was then used to control the electric motor.

To make it easier to analyze the closed-loop system behavior, we chose to simplify the mechanical dynamics as much as possible without loosing biological relevance. We chose the Hill muscle model [13] because it is relatively simple and is widely used to represent the active and passive components of the force produced by muscle. The *behavior* of the Hill model is equivalent to the position of the mass as a function of time. The full Hill model is shown in Fig. 1 as the passive and active mechanical components, which also contain nonlinearities. The passive mechanics of this model create a third order system, and the use of a third order mechanical system complicates the analysis when testing our hypothesis about resonant frequency. To further simplify the analysis, we made $k_{\rm s} \gg k_{\rm p}$. Physiologically, this correlates to tendons that are much stronger than the passive elastic properties of the muscle and soft tissue. Under this assumption, the model reduces to a second order system described by

$$m\ddot{x} = -2k_{\rm p}x - 2b\dot{x} + (F_1 - F_2). \tag{2}$$

In the Laplace domain, the transfer function of this second-order system is

$$H(s) = \frac{\frac{1}{m}}{s^2 + \frac{\omega_{0\rm m}}{Q}s + \omega_{0\rm m}^2} \tag{3}$$

where $H(s) = X(s)/F(s)$ is the transfer function, $X(s)$ is the laplace transform of the position, $F(s)$ is the Laplace transform of the active force, m is the mass, $\omega_{0\rm m} = \sqrt{2k_{\rm p}/m}$ is the natural frequency, and $Q = \omega_{0\rm m}m/2b$ is the quality factor. The magnitude and phase of the transfer function is given by

$$|H(j\omega)| = \frac{\frac{1}{\omega_{0\rm m}^2 m}}{\sqrt{\left(1 - \frac{\omega^2}{\omega_{0\rm m}^2}\right)^2 + \left(\frac{\omega}{\omega_{\rm om}Q}\right)^2}}$$
$$\angle H(j\omega) = -\arctan\left(\frac{\omega}{Q\omega_{0\rm m}\left(1 - \frac{\omega^2}{\omega_{0\rm m}^2}\right)}\right) \tag{4}$$

where ω is the frequency of the active force input. The resonant frequency is the frequency at which the magnitude response peaks. For $Q = \infty$, or zero damping, the resonant frequency is equivalent to $\omega_{0\rm m}$. However, if the damping is nonzero (i.e., all practical cases) the resonant frequency changes and is dependent upon the damping. The resonant frequency for any $Q > 1/\sqrt{2}$ is given by

$$\omega_{\rm r} = \omega_{0\rm m}\sqrt{1 - \frac{1}{2Q^2}}. \tag{5}$$

For $Q < 1/\sqrt{2}$ there is no peak in the magnitude response, but the natural frequency, $\omega_{0\rm m}$, remains a system property.

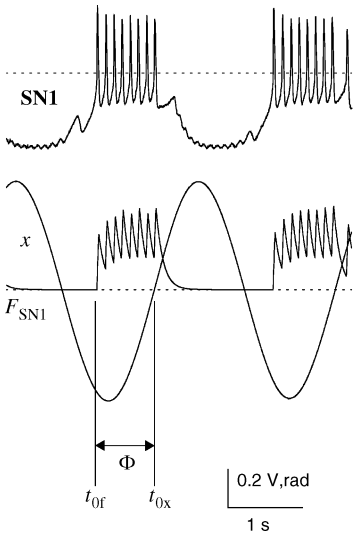

Fig. 3. The active force generated by the CPG. The top trace is the membrane potential of neuron SN1, and the dashed line indicates the threshold voltage for spike detection. The bottom trace is the force signal that is calculated by filtering the detected spikes. The force signal for SN2 is similar but shifted in phase. The dashed line indicates a value of zero active force. The position signal, x, is also shown superimposed on top of the $F_{\rm SN1}$ signal. The dashed line for the position signal represents the resting position. The zero-phase points for the position and CPG are denoted by $t_{0\rm f}$ for $F_{\rm SN1}$ and $t_{0\rm x}$ for the position signal. Φ is the phase difference between $F_{\rm SN1}$ and x.

The active forces, F_1 and F_2, generated by the muscles were calculated from the membrane potentials of SN1 and SN2 as shown in Fig. 3. The membrane potentials were rectified above a threshold voltage and the resulting waveforms were filtered with a first-order low-pass filter. This filter represents the transformation of the motor neuron action potentials to the active force produced by the muscle [14]. The time constant of the filter was 100 ms, which approximated the observed minimum spiking period. The force waveform illustrates the summation of action potentials to tetanus due to the difference in time constants between the filter and the action potentials. The force for each neuron was computed separately and the total active force is given by $F_{\rm T} = F_1 - F_2$.

To simplify the model, we did not include the nonlinearities of the length and velocity dependencies of the muscle when calculating the active force. The length approximation assumes the muscle is neither overly stretched or compressed [13]. The velocity approximation assumes the muscle is either stretched or compressed at relatively high velocities. The net effect of these approximations is an over- or underestimation of the active force, which will change the amplitude of the oscillations for rhythmic movements. However, these changes should not impact the qualitative results of our model.

Because the mass and the motor are physical entities, they add nonlinear friction components to the dynamics. These components were significantly impacting our analysis. Thus, we added a negative damping term that saturated at high velocities to 2 to make the system more linear for smaller displacements. This term is given by

$$F_{\rm nd} = B_{\rm nd} \tanh\left(S_{\rm nd}\frac{dx}{dt}\right) \tag{6}$$

where $F_{\rm nd}$ is the force added to compensate for the nonlinearities, $B_{\rm nd}$ is the saturation value, and $S_{\rm nd}$ is the damping coefficient in the linear region.

The mathematical model of the mechanical components in Fig. 1 was implemented in software on the real-time control board to compute the total force acting on the mass. The calculated value of the force was then split into the magnitude, $|F_{\rm ms}|$, and sign. The $|F_{\rm ms}|$ set the duty cycle of a pulse-width modulated (PWM) signal, which determined the amount of torque produced by the electric motor. The sign of the force set the direction of the current going to the electric motor, which determined the direction of rotation [15]. An additional gain term was added so that $|F_{\rm ms}|$ did not saturate the PWM signal, which would create nonlinear behavior.

C. Implementing Sensory Feedback

The sensory feedback, as shown in Fig. 1, represents proprioceptive sensors that synapse onto the CPG. These sensors were implemented as mathematical models on the real-time control board using the measured position of the mechanical system. The value of the feedback synaptic current was then summed with synaptic currents from the reciprocal inhibition to create the total current injected into each silicon neuron.

Again, we wanted to keep the model for these sensors as simple as possible without loosing biological relevance. Proprioceptive sensors are typically unidirectional, have either mechanical or neural saturation, and produce signals relative to a natural resting state [1]. As shown in Fig. 1, the sensory feedback in our system models two unidirectional position sensors, each of which makes an ipsilateral synaptic connection to one of the CPG neurons. The output of the position sensors is a smooth signal that we assume is proportional to a spike frequency of a neuron. Thus, the position signals are used directly as the presynaptic input to the feedback synapses. We chose to use ipsilateral inhibition as shown in Fig. 1 because it is biologically relevant and produced the most stable behavior due to the negative feedback [1].

The feedback synaptic current is calculated with the same model that was used for the reciprocal inhibitory synapses (1a). However, for the feedback synapses we ignore the synaptic time constants because they are at least an order of magnitude smaller than the mechanical time constants, and thus will not have an impact on the current. The feedback synaptic currents are give by

$$I_{\rm fb1} = \bar{g}_{\rm fb}\tanh(S_{\rm fb}(x_{\rm s1} - X_{\rm th}))(E_{\rm fb} - V_{\rm SN1}) \tag{7a}$$
$$I_{\rm fb2} = \bar{g}_{\rm fb}\tanh(S_{\rm fb}(x_{\rm s2} - X_{\rm th}))(E_{\rm fb} - V_{\rm SN2}) \tag{7b}$$

where $I_{\rm fb1}(I_{\rm fb2})$ is the feedback current for SN1(SN2), $\bar{g}_{\rm fb}$ is the maximal synaptic conductance, $S_{\rm fb}$ is the slope of the activation function where the sensor signal is zero, $X_{\rm th}$ is the position threshold that can provide hysteresis in the sensors, $x_{\rm s1}(x_{\rm s2})$ is the signal from the sensor for SN1(SN2), $E_{\rm fb}$ is the reversal potential of the feedback synapse, and $V_{\rm SN1}(V_{\rm SN1})$ is the membrane potential. The feedback connectivity is determined by how the sensor signals are paired with the membrane potentials in (7b). The reversal potential determines whether the feedback is excitatory or inhibitory. The two unidirectional position sensors, $x_{\rm s1}(x_{\rm s2})$, are created by half-wave rectifying the position signal in each direction relative to the resting state. The resting state for the sensor is the state in which the muscles are not actively producing force and no external forces are acting on the mass.

TABLE I
CANONICAL VALUES FOR THE MECHANICAL SYSTEM PARAMETERS AND FEEDBACK SYNAPTIC PARAMETERS

$k_{\rm s}$	100
$k_{\rm p}$	set by $\omega_{0\rm m}$ and Q
b	set by $\omega_{0\rm m}$ and Q
$B_{\rm nd}$	2.112
$S_{\rm nd}$	0.25
$\bar{g}_{\rm fb}$	0.4 nS
$S_{\rm fb}$	5.0
$E_{\rm fb}$	0.5 V
$X_{\rm th}$	0.0 rad

D. Characterizing the System

In order to study this system we defined a set of parameters to create a canonical behavior, to which we compared our other results. We determined previously a set of parameters for the silicon-neuron CPG to produce a typical bursting pattern (see Appendix) [9]. The canonical values for the mechanical and sensory feedback components are displayed in Table I. To facilitate the testing of our hypothesis, the parameters, $k_{\rm p}$ and b, were set by specifying the values for $\omega_{0\rm m}$ and Q in the simulation. We set $k_{\rm s} \gg k_{\rm p}$ for all practical values of Q and $\omega_{0\rm m}$. The negative damping parameters, $B_{\rm nd}$ and $S_{\rm nd}$, were set to optimize linearity at small amplitudes. The value of the feedback synaptic conductance, $\bar{g}_{\rm fb}$, was chosen because it was the minimum value that created stable oscillations over the range of $0.1 \leq \omega_{0\rm m} \leq 0.5$ Hz. This range of $\omega_{0\rm m}$ was chosen because it matched the range of burst periods that was possible from the half-center oscillator as the intrinsic neuron parameters were varied about their canonical values [9]. The value of $S_{\rm fb}$ was chosen so that the activation function saturated at a position angle of approximately 1 rad. $E_{\rm fb}$ was chosen to create inhibitory synapses and $X_{\rm th} = 0$ so that the sensory feedback would not have hysteresis.

In addition to choosing a canonical parameter space, there was no guarantee that the mechanical parameters, $\omega_{0\rm m}$ and Q, would accurately describe the physical behavior of the system because of the nonlinearities and additional parameters introduced by the dc motor and the coupling to the mass. Therefore, we measured the frequency response of the mechanical section in isolation from the rest of the system and for different values of Q. The resulting data are displayed in Fig. 4, which suggests that the mechanical system is sufficiently linear in the frequency range of interest from 0.1–0.5 Hz.

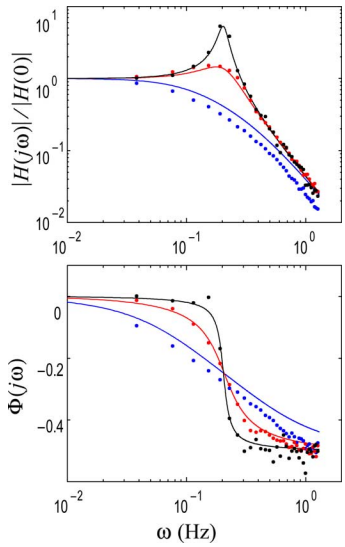

Fig. 4. Results from measuring the impulse response of the isolated mechanical system. The effective values of ω_{0m} and Q were extracted from the data via curve fits to the inverse laplace transform of (3). $\omega_{0m} = 0.2$ for all data. The three different responses are parameterized by $Q = 0.4$ for the overdamped case, $Q = 1.5$ and $Q = 5.2$ for the underdamped cases.

III. Developing a Steady-State Frequency Model for the Closed-Loop System

To test our hypothesis, we first determined how the steady-state frequency is created in the closed-loop system. Our results show that this frequency is determined by the phase properties of the CPG and mechanical systems. While the phase properties of a linear mechanical system are well-defined, those of the nonlinear CPG are not. We first characterize the CPG's phase curves in the open-loop system. We then use this relationship to develop an empirical model that explains the steady-state oscillation frequency in the closed-loop system.

A. Analysis of the Sensory Feedback

To better understand the closed-loop system, we first analyzed the open-loop response of the CPG by measuring the "transfer function" between the feedback synaptic input and the neural signals. The open-loop system was created by disconnecting the position sensors from the feedback synapses and applying a sinusoidal input signal instead. A sinusoid was used because it resembles the position oscillations of the closed-loop system. The frequency and amplitude of the sinusoid were varied systematically and the corresponding amplitude and phase shift of the neural oscillations were measured.

To quantify the phase difference the system must be synchronized and there must be a zero-phase point defined for each signal. Fig. 3 illustrates the zero phase points and how the phase difference was measured. The zero-phase point for the sinusoidal feedback signal was defined at zero radians[1] with a positive derivative (shown as t_{0x}). The zero-phase point for the CPG was defined as the first spike of each burst of the membrane potential of SN1 (shown as t_{0f}). SN1 was chosen because it drives the position positive, which correlates to the zero phase point of the feedback signal. The spikes were detected with a threshold of 1 V, and the first spikes of the burst periods were detected with a time threshold of 1 sec after the last spike from the previous burst period. For the closed-loop system we use the half-center oscillator (CPG) signal as the reference. Therefore, we measured the phase difference relative to this point as $\Phi = (t_{hc} - t_{fb})/T$, where Φ is the phase difference, t_{hc} is the time of the zero phase point of the half-center oscillator that occurs before the corresponding zero phase point of the feedback signal, t_{fb}, and T is the period of the oscillations.

Fig. 5(A) and (B) displays the phase response of the half-center oscillator with respect to frequency and amplitude of the feedback signal. For clarification, we define four new terms: 1) ω_{hc} is the burst frequency of the half-center oscillator in isolation from any external synaptic inputs; 2) ω_{in} is the frequency of the input signal that was applied to the feedback synapses; 3) α_{in} is the amplitude of the input signal; 4) ω_{sys} is the system frequency either in the open-loop or closed-loop configuration.

The data displayed in Fig. 5 define approximately the parameter space in which the CPG synchronized to the input signal (i.e., $\omega_{sys} = \omega_{in}$). We found that synchronization was dependent upon both the frequency of the input relative to the CPG and the amplitude of the input. When $\omega_{in} > \omega_{hc}$ the feedback synaptic current is introduced in the spiking part of the burst period. As a result, the spiking is subdued and the bursting transitions into the inhibited state, thus advancing the state of the CPG oscillations. When $\omega_{in} < \omega_{hc}$ the feedback is introduced in the inhibited part of the burst period, augmenting the reciprocal inhibition in the CPG and delaying the phase of the CPG oscillations. Fig. 5(B) illustrates the relationship between the input's frequency and the steady-state phase difference. The linear nature of this frequency-phase relationship for a given amplitude indicates that there is a constant time delay between the onset of the feedback and the termination of spiking [shown by t_{dl} in Fig. 5(C) and (D)]. The frequency–phase curves for the different amplitudes intersect at the natural frequency of the half-center oscillator. The phase difference at this frequency is slightly less negative than -0.5 $(\mathrm{rad}/2\pi)$ because the duty cycle is not exactly 50%.

The input's amplitude changes the magnitude of the feedback synaptic current, which directly affects the amount of phase advance or delay of the CPG oscillations. Fig. 5(A) and (B) illustrates the relationship between the input amplitude and the synchronization of the CPG to the input. First, the time delay, t_{dl}, is directly dependent upon the amplitude of the input. Larger amplitudes generate larger feedback synaptic currents that can more quickly inhibit spiking or create longer duration inhibited states, thus creating greater phase advances or delays in the CPG oscillations. Thus, for synchronization to occur at frequencies that are significantly different from ω_{hc}, larger input amplitudes are required as shown in the data. Second, once the amplitude is large enough to saturate the feedback synaptic conductance, further increases in amplitude have no change in effect. At such large amplitudes the feedback synaptic conductance changes

[1]As mentioned in Section II-C, the feedback signal represents the firing frequency of sensory neurons and we are assuming that this firing frequency is linearly proportional to the position. To make the analysis easier, we set the proportionality constant to 1. As such, the feedback signal is equivalent to the position of the mechanical system. Because the mechanical position is rotational, the position is expressed in radians. Thus, the units for the amplitude of the feedback signal are in radians.

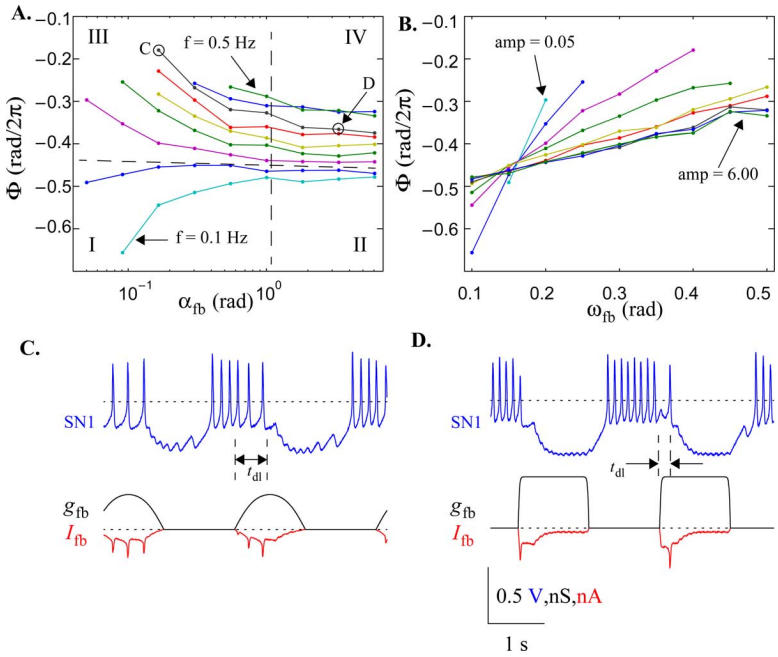

Fig. 5. Open-loop phase response with a sinusoid of given amplitude and frequency applied as the feedback signal. Each datum in (A) and (B) represents the average phase difference over a 30-s interval. (A) Phase difference with respect to the amplitude of the feedback signal and parameterized by linearly changing frequency bounded by the indicated values. The horizontal dashed line indicates the phase difference for $\omega_{\rm in} = \omega_{\rm hc} \approx 0.17$ Hz. The vertical dashed line indicates the amplitude at which the feedback conductance begins to saturate. (B) Phase with respect to the frequency of the feedback signal and parameterized by amplitude. (C) and (D) Time series data corresponding to the circled data points from (A). The dashed line for SN1 indicates the threshold voltage for spike detection. The dashed line for $I_{\rm fb}$ and $g_{\rm fb}$ indicates a value of 0 nA and 0 nS. The scale bars at the bottom of the figure are for the corresponding column of traces.

very quickly to it's maximal value [see Fig. 5(D)], making the steady-state phase difference constant at approximately the duty cycle of the half-center oscillations. When $\omega_{\rm in} > \omega_{\rm hc}$, the large amplitude feedback terminates spiking earlier in the burst period and then augments the reciprocal inhibition for a given period of time. The result is an extra amount of time that the neurons are inhibited and a decrease in the duty cycle, and consequently, phase. When $\omega_{\rm in} < \omega_{\rm hc}$ the phase shift saturates at approximately $-0.5\ \mathrm{rad}/2\pi$ because the feedback dominates the inter-burst inhibition instead of the reciprocal inhibition of the CPG. This large amplitude effect can be seen in Fig. 5(A) in the data that are to the right of the vertical dashed line. The phase is relatively constant for a given frequency, and as the frequency increases the phase decreases.

B. The Steady-State Frequency Model

The steady-state frequency, $\omega_{\rm sys}$, of the closed-loop system is based on the phase responses of the mechanical system, described by (4), and the half-center oscillator, described in Fig. 5. The phase response of the mechanical system defines the relationship between the input force and the resulting position of the mechanical system. In the previous section we defined the open-loop phase relationship to be between the half-center oscillations and the position of the mechanical system. When the loop is closed, the phase response of the CPG and mechanical system must sum to zero. Because we defined the open-loop phase response of the CPG as a negative phase, the CPG's phase response and the mechanical system's phase response must be the same. Therefore we can plot the phase relationships of both the CPG and the mechanical system on the same axes (as shown in Fig. 6) and the intersection of the two curves should indicate the resulting steady-state frequency.

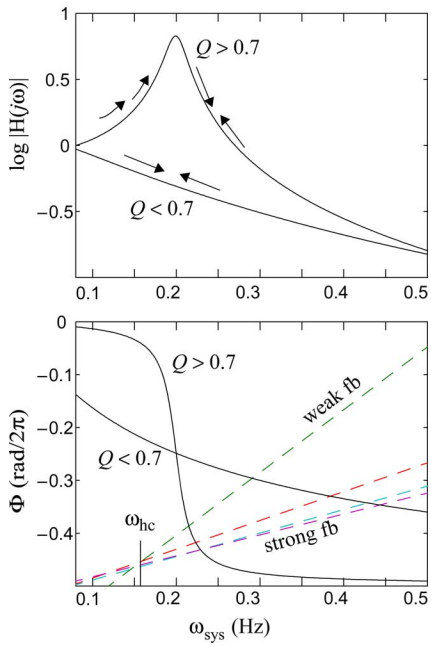

Fig. 6. An illustration of the steady-state frequency model. The bode plot of the mechanical system is plotted for $Q > 1/\sqrt{2}$ and $Q < 1/\sqrt{2}$. For the top figure, the arrows pointing in opposite directions indicate regions of negative feedback with respect to the amplitude response. The arrows pointing in the same directions indicate regions of positive feedback. The CPG's phase curves are denoted by the dashed lines, which are parameterized by the strength of the feedback. These particular lines were calculated using linear regression on the data in Fig. 5(B).

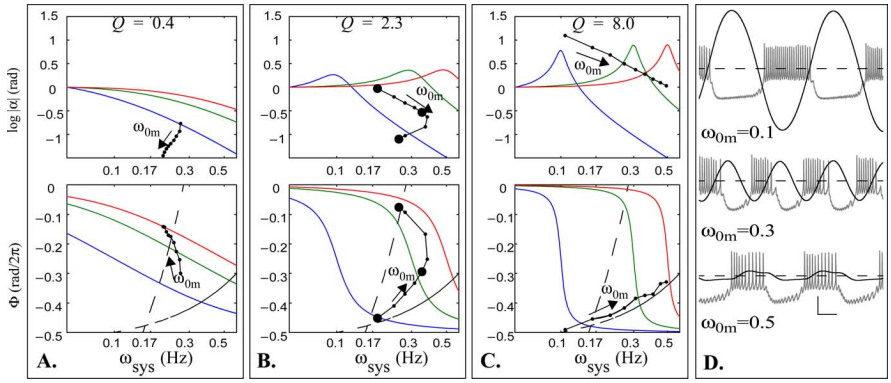

Fig. 7. (A)–(C) System frequency, position amplitude, and phase data with respect to variation of $\omega_{0\mathrm{m}}$ for three different fixed values of Q, which are indicated above each column. The data are denoted by the black-dotted curves, for which each point was measured at a different value of $\omega_{0\mathrm{m}} = [0.1, 0.15, 0.2, 0.25, 0.3, 0.35, 0.4, 0.45, 0.5]$ Hz and the arrows indicate the direction of increasing $\omega_{0\mathrm{m}}$. The smooth curves represent the frequency response of the mechanical system for three different values of $\omega_{0\mathrm{m}}$ (left is 0.1 Hz, center is 0.3 Hz, and right is 0.5 Hz). The magnitude responses of the mechanical system are normalized to the lowest-frequency value. The natural CPG frequency, $\omega_{\mathrm{hc}} = 0.17$ Hz. The dashed lines indicate the two extremes of the feedback phase curves from Fig. 5(B). (D) Time series for three different values of $\omega_{0\mathrm{m}} = [0.1, 0.3, 0.5]$ Hz as indicated by the larger data points in B. The position signal (black) is superimposed on the membrane potential of SN1 (gray). The dashed lines indicate both the threshold voltage for calculation of active force production and the position of 0 rad. The scale bars at the bottom indicate a time length of 1 s and an amplitude of 0.25 V or 0.25 rad accordingly.

In Fig. 6, the CPG's phase curves are parameterized by weak–strong feedback instead of amplitude. This transition was based on qualitative experimentation, which revealed that the slope of these CPG phase curves was based on the "strength" of the feedback synapses. *Strong* feedback is the ability to terminate spiking almost instantly [see Fig. 5(D)], and *weak* feedback causes the spike frequency to decrease gradually [see Fig. 5(C)]. While the position amplitude affects the feedback strength directly, there are other factors such as the maximal conductance parameter of the synapses and the intrinsic neuron dynamics that also affect the strength.

As shown in Fig. 6, the frequency response of the mechanical system also affects the position amplitude. This dependency creates a complex interaction between the CPG and the mechanical system in which the phase response determines the frequency, the frequency affects the position amplitude, and the position amplitude affects the phase. This interaction is further complicated because the mechanical system's amplitude response changes with respect to Q. For $Q < 1/\sqrt{2}$, the mechanical system is overdamped and there is no resonant peak in the magnitude of the frequency response. For this case, if the system frequency increases, the position amplitude will decrease. The decrease in amplitude is represented by a greater slope in the CPG's phase curve, as shown in Fig. 6. As the slope increases, the intersection of the two curves occurs at a lower frequency. Thus, an increase in frequency is countered by a subsequent decrease in frequency due to the decrease in amplitude as shown by the opposing arrows in Fig. 6. For $Q > 1/\sqrt{2}$, the mechanical system is underdamped, and an increase in the system frequency will have different effects on the amplitude depending on the relationship between the system frequency and the resonant frequency, ω_{r}. For $\omega_{\mathrm{sys}} < \omega_{\mathrm{r}}$, the amplitude increases with respect to frequency as shown in Fig. 6. The increasing amplitude will cause the system frequency to increase further because the slope of the CPG's phase curve decreases. Thus the system frequency will continue to increase until it becomes greater than or equal to ω_{r} as shown by the arrows pointing in the same direction. For $\omega_{\mathrm{sys}} > \omega_{\mathrm{r}}$, the amplitude decreases with respect to frequency as shown in Fig. 6. The decreasing amplitude will cause the system frequency to decrease, countering any increase in system frequency.

IV. Analysis of Steady-State Oscillations in the Closed-Loop System

The steady-state frequency model can be used to describe the behavior of the closed-loop system as different parameters are varied. The mechanical parameters correlate to biological changes such as growth and injury, and co-contraction, which can immediately change the stiffness of a joint [5]. The intrinsic neuron parameters are often used to model the modulation of neural activity in biological systems [16]. We show that our hypothesis is valid under certain circumstances, and also use the steady-state frequency model to describe the general effects of sensory feedback on rhythmic movements.

A. Variation of $\omega_{0\mathrm{m}}$ and Q

We first explored the closed-loop system by varying the natural frequency of the mechanical system, $\omega_{0\mathrm{m}}$, and the quality factor, Q, of the mechanical system and the results are displayed in Fig. 7.[2] This data can be described using the steady-state frequency model that was presented in Fig. 6. Two primary mechanisms interact to change the frequency at which the phase curves intersect. First, as $\omega_{0\mathrm{m}}$ is increased, the position amplitude decreases according to (4) and the mechanical system's phase curve is shifted to the right. Second, as the position amplitude decreases, the magnitude of the feedback decreases, effectively increasing the slope of the CPG's phase curve.

Fig. 7(A) illustrates the case for an overdamped mechanical system. The position amplitude for $\omega_{0\mathrm{m}} = 0.1$ Hz is approximately 0.2 rad, and continues to decrease with increasing $\omega_{0\mathrm{m}}$. The corresponding increase in the slope of the CPG's phase curve causes the system frequency to decrease despite the shift of the

[2]If $Q > 1/\sqrt{2}$ and is constant, then varying $\omega_{0\mathrm{m}}$ is equivalent to varying ω_{r} as described in (5).

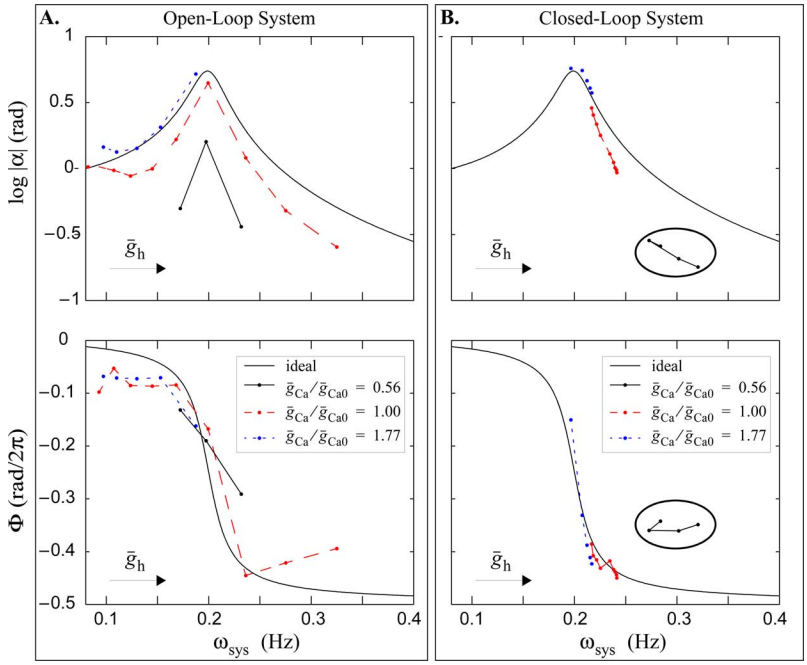

Fig. 8. System behavior with respect to the combined variation of the intrinsic neuron parameters $\bar{g}_{\rm h}$ and $\bar{g}_{\rm Ca}$. (A) Illustrates the open-loop amplitude and phase data with respect to system frequency. (B) Illustrates the closed-loop amplitude and phase data with respect to system frequency. The data are plotted on the Bode Plot of the mechanical system for which the parameters $\omega_{0\rm m} = 0.2$ Hz and $Q = 6.0$. The calculated amplitude response of the mechanical system was normalized to the dc value; however, the system data were not normalized, and are plotted as the logarithm of the measured value. In general, increasing $\bar{g}_{\rm h}$ increases the system frequency as shown by the arrows in the lower left of each plot. The three groups of data in each plot represent three different values of $\bar{g}_{\rm Ca}$ as specified by the legends.

mechanical system's phase curve. The large gap between the mechanical system's phase curve and the datum for $\omega_{0\rm m} = 0.1$ Hz is due to a decrease in the duty cycle of the half-center oscillations.

Fig. 7(B) illustrates the case for a moderately underdamped mechanical system. Because of the increase in Q, the position amplitude is slightly larger than for the overdamped case. As such, the system frequency follows the intersection of the curves as the mechanical system's frequency response is shifted. However, for $\omega_{0\rm m} > 0.35$ Hz, the amplitude decreases significantly as shown in Fig. 7(B) and (D). As a result, the feedback becomes weaker and the intersection of the two phase curves occurs at lower frequencies because of the increasing slope of the CPG's phase curve. As the slope continues to increase the system frequency becomes closer to the natural half-center frequency. Fig. 7(D) illustrates these effects in the time series of the data. For small amplitude oscillations, the feedback has very little influence on the CPG and thus the frequency of oscillations is determined by the CPG and the phase relationship by the mechanical system.

Fig. 7(C) illustrates the case for a highly underdamped mechanical system. Although the amplitude decreases with $\omega_{0\rm m}$, the feedback conductance is saturated because the position amplitude is greater than 1 rad for all values of $\omega_{0\rm m}$. As a result, the data lie along the CPG's phase curve for the saturated feedback conductance, and the change in system frequency is dependent primarily upon the shifting of the mechanical system's phase curve.

Analysis of Fig. 7 reveals that, for high Q the system can synchronize to the mechanical resonant frequency. The mechanical system's phase curve is centered around $\omega_{\rm r}$, and for high Q, the slope is very steep. If the CPG's phase curve intersects the mechanical system's phase curve on the central "vertical" portion, the system frequency will be close the mechanical resonant frequency. At lower values of Q the slope of the mechanical system's phase curve is much less. Under these conditions, the mechanical system and CPG phase curves can intersect over a much wider range of frequencies.

B. Effects of the Neuron Parameters on the Steady-State Frequency

In the previous section, we assumed that the bursting properties of the neurons were fixed. In this section, we show how the neuron dynamics affect the steady-state frequency model by varying the neuron parameters while fixing the mechanical parameters. In general, varying the neuron parameters impacts the burst frequency and spike frequency of the natural oscillations of the half-center oscillator [17]. According to our model, changes in burst period shift the CPG's phase curve horizontally. Changes in spike frequency impact the strength of the feedback synapses and thus affect the slope of the CPG's phase curve. In particular, the maximal conductances $\bar{g}_{\rm h}$ and $\bar{g}_{\rm Ca}$ are varied because they model the effects of neuromodulators and were found to produce the broadest range of burst periods and spike frequencies [9]. We varied these parameters for the cases of a highly underdamped (Q = 6.0) and an overdamped (Q = 0.4) mechanical system. For each case, $\omega_{0\rm m} = 0.2$ Hz, which is similar to the intrinsic burst frequency of the half-center oscillator at the canonical parameters.

Fig. 8 illustrates how the parameters $\bar{g}_{\rm h}$ and $\bar{g}_{\rm Ca}$ affect the system behavior for both the open-loop[3] Fig. 8(A) and closed-

[3]The open-loop system was created by disconnecting the sensory feedback from the half-center oscillator.

loop Fig. 8(B) system. The effects of varying these maximal conductances on the burst period, spike frequency, and duty cycle of the half-center oscillations were measured previously [9]. Increasing $\bar{g}_{\mathrm{Ca}}$ increases relatively linearly both the spike frequency and burst period. Increasing $\bar{g}_{\mathrm{h}}$ decreases the burst period nonlinearly and decreases slightly the spike frequency [9]. The open-loop data also show that the amplitude and phase of the position signal are relatively well described by the frequency response of the mechanical system. The vertical offset of the three data traces in Fig. 8(A) is due to a decrease in spike frequency for decreasing $\bar{g}_{\mathrm{Ca}}$. The decreased spike frequency decreases the active force generated by the muscle model, resulting in a smaller position amplitude. In contrast, the spike frequency is relatively independent of $\bar{g}_{\mathrm{h}}$, and as a result, the data tend to follow the magnitude and phase response of the mechanical system.

Applying the steady-state frequency model to Fig. 8(B) shows that the feedback causes the system to oscillate at approximately the mechanical resonant frequency. As the maximal conductances are varied, they change the slope and location of the CPG's phase curve. Because the mechanical system's phase curve has a vertical component (see Section IV-A), the intersection of the two phase curves is most likely to occur near the mechanical resonant frequency.

For $\bar{g}_{\mathrm{Ca}}/\bar{g}_{\mathrm{Ca0}} = 1.77$, the half-center bursting has very strong plateau potentials, which create a lower burst frequency and higher spike frequency. Because of these bursting properties, the feedback is insufficient to terminate spiking even if the conductance is saturated. This behavior is roughly equivalent to weak feedback and can be represented by increasing the slope of the CPG's phase curve. The decrease in ω_{hc} is equivalent to shifting the CPG's phase curve to the left. These two effects cause the intersection of the mechanical and CPG phase curves to occur near the mechanical resonant frequency.

For $\bar{g}_{\mathrm{Ca}}/\bar{g}_{\mathrm{Ca0}} = 1.00$, the plateau potentials are not as strong, which strengthens the feedback and increases the burst frequency. These effects correlate to a rightward shift and a decrease in the slope of the CPG's phase curve. The resulting intersection of the phase curves occurs at a higher system frequency and the phase difference is closer to $-0.5\ \mathrm{rad}/2\pi$.

For $\bar{g}_{\mathrm{Ca}}/\bar{g}_{\mathrm{Ca0}} = 0.56$, the CPG produced anti-phasic bursting only when combined with values of $\bar{g}_{\mathrm{h}}$ that were also below canonical values. The result of this parameter set was weak plateau potentials and reduced ability of the cell to recover from inhibition. Together, these effects strengthened the inhibitory sensory feedback, which would cause the intersection of the phase curves to occur at a higher system frequency and larger phase difference. These data are indicated by the oval in Fig. 8(B) and show that the system frequency is higher as predicted by our model, but that the phase is offset from the ideal mechanical phase curve. This offset is correlated with a 10% reduction in the duty cycle of the CPG oscillations as shown in Fig. 9. This data shows that the position is phase shifted to correlate with the end of a burst. This phase shift would lie along the mechanical system's phase curve at $\Phi \approx -0.5\ \mathrm{rad}/2\pi$ if the duty cycle of the CPG were 50%.

These data indicate that, if the mechanical system can be characterized with a higher Q value, there are two conditions that will cause the closed-loop system to oscillate near the mechanical resonant frequency: 1) if the natural frequency of the CPG is less than the mechanical resonant frequency and the feedback is of the appropriate strength or 2) if the natural frequency of the CPG is higher than the mechanical resonant frequency and the feedback is relatively strong. It is often observed that isolated CPGs have slower frequencies than the movements of intact animals [11]. To create this condition, perhaps there is some form of long-term potentiation of the synapses within the CPG that is guided by the sensory feedback.

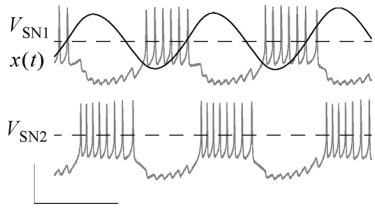

Fig. 9. Time series for the circled data in Fig. 8. The position signal (black) is superimposed on the membrane potential of SN1 (gray). The dashed lines indicate both the threshold voltage for calculation of active force production and the position of 0 rad. The scale bars at the bottom indicate a time length of 2 s and an amplitude of 0.5 V or 0.2 rad accordingly.

Many biological systems, such as insect walking, can be described with overdamped mechanics ($Q < 0.707$) [18], [19]. Increasing the damping decreases the amplitude of movement for a given force input (4) and produces a mechanical phase curve that is monotonically decreasing. Because of these properties, the intersection of the two phase curves can occur over a much broader range of frequencies [compare Figs. 8(B) and 10(B)]. As such, the natural frequency of the CPG has a greater impact on the closed-loop system frequency. Fig. 10 displays the open-loop and closed-loop system data for the case of an overdamped mechanical system, $Q = 0.4$. The burst properties are varied in the same manner as was done for the underdamped system.

For $\bar{g}_{\mathrm{Ca}}/\bar{g}_{\mathrm{Ca0}} = 1.77$, the large plateau potentials, high spike frequency, and small amplitude of movement creates very weak feedback. As a result, the CPG's phase curve is almost vertical and the closed-loop system frequency is not significantly different from the open-loop frequency for smaller values of $\bar{g}_{\mathrm{h}}$. For larger values of $\bar{g}_{\mathrm{h}}$, the feedback does have some impact because the closed-loop system is capable of oscillations that were not evident in the open-loop system. These oscillations arise because the larger $\bar{g}_{\mathrm{h}}$ values prevent the neurons from hyperpolarizing, which lowers the plateau potentials and makes the feedback stronger [9]. The stronger feedback implies a higher system frequency according to our model because of the reduced slope of the CPG phase curve. Fig. 10(B) shows that the system frequency increases with respect to increasing $\bar{g}_{\mathrm{h}}$.

For $\bar{g}_{\mathrm{Ca}}/\bar{g}_{\mathrm{Ca0}} = 1.00$ and $\bar{g}_{\mathrm{Ca}}/\bar{g}_{\mathrm{Ca0}} = 0.56$, the amplitude of movement is even smaller than it was for $\bar{g}_{\mathrm{Ca}}/\bar{g}_{\mathrm{Ca0}} = 1.77$ because of the lower spike frequencies. The smaller amplitudes create less feedback to the CPG. However, in these regions of the parameter space, the CPG's plateau potentials are not as large and so the feedback, while less, is stronger than it was for $\bar{g}_{\mathrm{Ca}}/\bar{g}_{\mathrm{Ca0}} = 1.77$. The stronger feedback causes the slope of the CPG's phase curve to decrease, resulting in

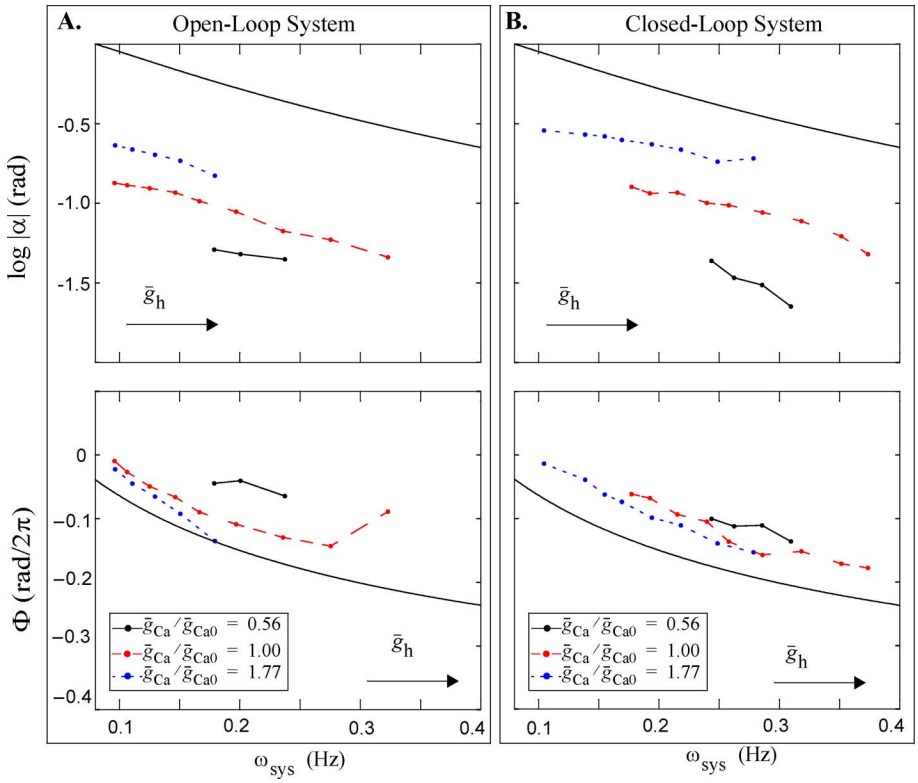

Fig. 10. Same format as the data presented in Fig. 8, except for this data set $Q = 0.4$. (A) Illustrates the open-loop amplitude and phase data with respect to system frequency. (B) Illustrates the closed-loop amplitude and phase data with respect to system frequency.

a closed-loop system frequency that is higher than the open-loop frequency. This result supports observations from biological studies showing that CPGs, when extracted from the nervous system, have slower frequencies than the movements of the intact animal [1]. Our steady-state frequency model predicts this phenomenon because the intersection of the two phase curves must occur at a frequency that is greater than the natural frequency of the half-center oscillator.

V. Conclusion

In this paper, we presented the implementation and analysis of a closed-loop system, consisting of a biologically realistic half-center oscillator, a second-order linear mechanical system, and position feedback. The half-center oscillator is constructed with two silicon neurons, each with six voltage-dependent conductances. The mechanical system consists of a physical mass driven by a dc electric motor. The motor is controlled by the CPG and the position of the mass is fed back to the CPG via ipsilateral inhibitory synapses. We studied the effects of the closed-loop system on the neuron dynamics of the CPG and developed a model for mechanisms that create a steady-state system frequency.

We were able to use this steady-state frequency model to define principles that may underlie biological rhythmic movement control. It is well established that sensorimotor feedback influences the motor patterns of CPGs, but the exact nature and purpose of the influence is unclear [1]. The results from this work describe a possible synergy that exists between the mechanical properties of the system, CPG, and sensory feedback.

Our model suggests that when the mechanical properties are more characteristic of an underdamped system, the resulting system frequency is influenced more by the mechanical resonance than the CPG. Movements such as running and hopping fit into this category because, for efficiency, the body takes advantage of the mechanical energy stored in the system. It has been suggested that the mechanical resonance is not a fixed property of a biological system and can be influenced significantly by activating muscles at particular phases of a rhythmic movement. As such, the phase of the movement cycle in which a muscle is activated determines whether it is used to store energy, dissipate energy, or actively produce force [19]. In addition, the co-contraction of an antagonist muscle pair can be used to stiffen the movement about a given joint, which changes the damping. These changes to the mechanical resonance set the overriding frequency of movement, while changes in the strength of the feedback or in the natural characteristics of the CPG vary the system frequency as slight deviations from this mechanical resonance. A number of physiological mechanisms including presynaptic facilitation, second messenger systems, and descending synaptic input to the CPG could underlie such neural changes on a short time scale.

In contrast, when the mechanical properties are more characteristic of an overdamped system, our model suggests that the resulting system frequency is influenced more by the CPG and the strength of the feedback than the mechanical properties. Movements such as walking and swimming fit into this category because a significant amount of damping is created either by the environment or the body itself to make the movements smooth

and controlled. In this scenario, our model suggests a novel mechanism for varying the frequency of movement. Namely, that the feedback strength could be adjusted instead of the natural frequency of the CPG. We indicated in Section IV-B that the "strength" of the feedback is determined by the relationship of the feedback synaptic efficacy to the complex dynamics of the CPG. Thus, any change in the efficacy of the feedback synapses will have a direct impact on this feedback strength. According to our model this change in feedback strength adjusts the slope of the CPG's phase curve, which corresponds to a change in the closed-loop system frequency. Physiologically, the feedback synaptic efficacy could be adjusted through a mechanism such as presynaptic facilitation or depression, which is often associated with the axons of sensory neurons. Such a control structure would make it much easier for higher neural centers to make fine adjustments of rhythmic movements than trying to directly control the natural frequency of a complex CPG.

One of the major goals of functional electrical stimulation (FES) is to restore the ability to walk, which is a rhythmic movement. A thorough understanding of the relationship between pattern generators and sensory feedback could improve the control strategies of FES systems. The results presented here suggest that, in addition to the motor units, the sensory feedback should be an important part of any control strategy to artificially illicit rhythmic movements.

In the sense that our model of the closed-loop system is based on equal phase relationships between the CPG and the mechanical system, it is independent of the complexity contained in that system. However, one of our goals was to understand the role that the complex neural dynamics might play in the control of rhythmic movements. We found that the neural dynamics fit into our model of the closed-loop system in that they impact the strength of the synaptic feedback and the shape of the CPG's phase curve. For example, for the same amount of feedback (i.e., same amplitude of movement), the feedback was weaker when the neurons exhibited strong plateau potentials.

We could change the neural complexity by changing the number of neurons in the CPG and/or the complexity of the individual neurons. Simpler neuron dynamics tend to express a less rich set of behaviors or have fewer state dependent behaviors [20]. It would seem likely that for less complex neurons, the feedback strength would be more predictable with respect to the individual neural dynamics. Changes to the complexity of the CPG and the neurons will also impact the shape of the CPG's phase curve. We plan to explore how these changes to the phase curve impact the synchronization of the system.

There were several parameters of this system that we have not yet explored. One of the more obvious is the feedback synaptic conductance, which has a direct impact on the strength of the feedback. As shown in Fig. 7, the system frequency is directly dependent on the amplitude of oscillations because of it's impact on feedback strength. In biology, the feedback conductance is likely controlled through some form of presynaptic facilitation or depression. According to our model, one reason for coordination between the feedback gain and the musculoskeletal mechanics could be to help maintain movement at a given frequency. Another aspect that we wish to address in the future is the effects of noise, mismatch, and imperfections. We purposely stifled such properties as much as possible to make the analysis tractable. However, this system is ideally suited for studying these properties because they are an inherent part of the system. We plan to use this system to study how adaptation and modulation are used in biology to work around these imperfections [21].

APPENDIX

The equations that describe the silicon neurons are fundamentally similar to the Hodgkin-Huxley formalism. These equations are summarized with the following equations:

$$C\frac{dV}{dt} = I_{\mathrm{Na}} + I_{\mathrm{P}} + I_{\mathrm{K1}} + I_{\mathrm{K2}} + I_{\mathrm{Ca}} + I_{\mathrm{h}} + I_{\mathrm{leak}} \quad (8)$$

$$I_{\mathrm{leak}} = \bar{g}_{\mathrm{leak}}(E_{\mathrm{leak}} - V) \quad (9)$$

$$I_j = \bar{g}_j m_j^{\kappa} h_j (E_j - V) \quad (10)$$

$$I_j = \bar{g}_j m_j (E_j - V) \quad (11)$$

$$\frac{dm_j}{dt} = \frac{1}{\tau_{\mathrm{m}j}}(m_{\infty j}(V) - m_j) \quad (12)$$

$$\frac{dh_j}{dt} = \frac{1}{\tau_{\mathrm{h}j}}(h_{\infty j}(V) - h_j) \quad (13)$$

$$m_{\infty j}(V) = \frac{1}{1 + \exp(S_{\mathrm{m}j}(V_{\mathrm{m}j} - V)} \quad (14)$$

$$h_{\infty j}(V) = \frac{1}{1 + \exp(S_{\mathrm{h}j}(V_{\mathrm{h}j} - V)} \quad (15)$$

where C is the membrane capacitance, V is the membrane potential, and I is a current. For (10)–(15), the subscript $j \in$ [Na, P, K1, K2, Ca, h]. Equation (9) describes the leak current, for which $\bar{g}_{\mathrm{leak}}$ is the leak conductance and E_{leak} is the leak reversal potential. Equation (10) describes the current for the conductances Na, K1, and Ca, which are characterized with both an activation variable, m_j, and an inactivation variable, m_j. $\bar{g}_j$ is the maximal conductance and E_j is the reversal potential. The activation variable is raised to a fixed power of $\kappa \approx 0.7$ because of a property of the integrated circuits. Equation (11) describes the current for the conductances P, K2, and h, which have only an activation variable. Equation (12) and (13) describe the dynamics of the activation and inactivation variables. $\tau_{\mathrm{m}j}$ and $\tau_{\mathrm{h}j}$ are the activation and inactivation time constants, and $m_{\infty j}(V)$ and $h_{\infty j}(V)$ are the steady-state activation and inactivation functions. Equation (14) and (15) describe the steady-state functions as functions of the membrane potential. $S_{\mathrm{m}j}$ and $S_{\mathrm{h}j}$ represent the slopes of these functions and $V_{\mathrm{m}j}$ and $V_{\mathrm{h}j}$ represent the half-maximal potentials.

ACKNOWLEDGMENT

The authors would like to thank R. Calabrese and R. Nichols at Emory University for their review of this work and suggestions.

REFERENCES

[1] A. Cohen and D. Boothe, "Sensorimotor interactions during locomotion: Principles derived from biological systems," *Auton. Robot.*, vol. 7, no. 3, pp. 239–245, 1999.

[2] L. Goodman, M. Riley, S. Mitra, and M. Turvey, "Advantages of rhythmic movements at resonance: Minimal active degrees of freedom, minimal noise, and maximal predictability," *J. Motor Behavior*, vol. 32, no. 1, pp. 3–8, 2000.

[3] K. Holt, S. Jeng, R. Ratcliffe, and J. Hamill, "Energetic cost and stability during human walking at the preferred stride frequency," *J. Motor Behavior*, vol. 27, no. 2, pp. 164–178, 1995.
[4] N. Hatsopoulous, "Coupling the neural and physical dynamics in rhythmic movements," *Neural Computation*, vol. 8, pp. 567–581, 1996.
[5] C. Farley and O. Gonzalez, "Leg stiffness and stride frequency in human running," *J. Biomech.*, vol. 29, no. 2, pp. 181–186, 1996.
[6] C. Farley, J. Glasheen, and T. McMahon, "Running springs: Speed and animal size," *J. Exper. Biol.*, vol. 185, pp. 71–86, 1993.
[7] T. McMahon and G. Cheng, "The mechanics of running: How does stiffness couple with speed?," *J. Biomech.*, vol. 23, no. Suppl. 1, pp. 65–78, 1990.
[8] M. F. Simoni, G. S. Cymbalyuk, M. E. Sorensen, R. L. Calabrese, and S. P. DeWeerth, "A multiconductance silicon neuron with biologically matched dynamics," *IEEE Trans. Biomed. Eng.*, vol. 51, no. 2, pp. 342–354, Feb 2004.
[9] M. F. Simoni and S. P. DeWeerth, "Two-dimensional variation of bursting properties in a silicon-neuron half-center oscillator," *IEEE Trans. Neural Syst. Rehabil. Eng.*, vol. 14, no. 3, pp. 281–289, Sep. 2004.
[10] F. Nadim, O. Olsen, E. D. Schutter, and R. Calabrese, "Modeling the leech heartbeat elemental oscillator: I. Interactions of intrinsic and synaptic currents," *J. Computational Neurosci.*, vol. 2, pp. 215–235, 1995.
[11] S. H. Jezzini, A. A. Hill, P. Kuzyk, and R. L. Calabrese, "Detailed model of intersegmental coordination in the timing network of the leech heartbeat central pattern generator," *J. Neurophysiol.*, vol. 91, no. 2, pp. 958–977, Feb. 2004.
[12] A. Destexhe, Z. Mainen, and T. Sejnowski, "An efficient method for computing synaptic conductances based on a kinetic model of receptor binding," *Neural Computation*, vol. 6, pp. 14–18, 1994.
[13] Y.-C Fung*, Biomechanics: Mechanical Properties of Living Tissues*. New York: Springer-Verlag, 1993, ch. Skeletal Muscle, pp. 392–424.
[14] G. Rab*, Muscle*, J. Rose and J. Gamble, Eds. Baltimore, MD: Williams & Wilkins, 1994.
[15] S. P. DeWeerth, "Converting spatially encoded sensory information to motor signals using analog vlsi circuits," *Auton. Robot.*, vol. 2, no. 2, pp. 93–104, 1995.
[16] L. Abbott and G. LeMasson, "Analysis of neuron models with dynamically regulated conductances," *Neural Computation*, vol. 5, no. 6, pp. 823–843, 1993.
[17] V. Brezina, I. V. Orekhova, and K. R. Weiss, "The neuromuscular transform: The dynamic, nonlinear link between motor neuron firing patterns and muscle contraction in rhythmic behaviors," *J. Neurophysiol.*, vol. 83, pp. 207–231, 2000.
[18] J. Dean, T. Kindermann, J. Schmitz, M. Schumm, and H. Cruse, "Control of walking in the stick insect: From behavior and physiology to modeling," *Auton. Robot.*, vol. 7, no. 3, pp. 271–288, 1999.
[19] M. H. Dickinson, C. T. Farley, R. J. Full, M. A. R. Koehl, R. Kram, and S. Lehman, "How animals move: An integrative view," *Science*, vol. 288, pp. 100–106, 2000.
[20] R. Butera, "Mulitrhythmic bursting," *Chaos*, vol. 8, no. 1, pp. 274–284, 1998.
[21] M. Simoni and S. DeWeerth, "Adaptation in an a VLSI model of a neuron," *IEEE Trans. Circuits Syst.-II: Analog Digit. Signal Process.*, vol. 46, no. 7, pp. 967–970, 1999.

Mario F. Simoni (S'92–M'96) received the B.S. degree in electrical engineering from Parks College, St. Louis University, St. Louis, MO, and the M.S.E.E. and Ph.D. degrees from the Georgia Institute of Technology, Atlanta, GA.

He is currently an Assistant Professor of Electrical and Computer Engineering at Rose-Hulman Institute of Technology, Terre Haute, IN. His research interests include the development of integrated circuit models of neurons for use in biomedical and robotics applications and teaching pedagogy for electronics, integrated circuit design, and biomedical engineering.

Stephen P. DeWeerth (S'85–M'90–SM'03) received the M.S. degree in computer science and the Ph.D. degree in computation and neural systemsfrom the California Institute of Technology, Pasadena, in 1987 and 1991, respectively.

He is a Professor in the Wallace H. Coulter Department of Biomedical Engineering and in the School of Electrical and Computer Engineering, the Georgia Institute of Technology, Atlanta, and at the Emory University School of Medicine, Atlanta, GA. His research focuses on the implementation of neuromorphic electronic and robotic systems, the development of neural interfacing technologies, and the study of the biological control of movement.